http://dx.doi.org/10.5012/bkcs.2013.34.2.384

Roles of Fluorine-doping in Enhancing Initial Cycle Efficiency and SEI Formation of Li-, Al-cosubstituted Spinel Battery Cathodes

Cao Cuong Nguyen,[†] Young-San Bae,[†] Kyung-Ho Lee,[†] Jin-Woo Song,[‡,§] Jeong-Hye Min,[‡] Jong-Seon Kim,[†] Hyun-Seok Ko,[§] Younkee Paik,[#] and Seung-Wan Song[†,‡,*]

[†]*Department of Fine Chemical Engineering & Applied Chemistry,* [‡]*Graduate School of Green Energy Technology, Chungnam National University, Daejeon 305-764, Korea.* [*]*E-mail: swsong@cnu.ac.kr*
[§]*POSCO ES Materials, Gumi 730-853, Korea*
[#]*Korean Basic Science Institute, Daegu 702-701, Korea*
Received August 27, 2012, Accepted November 7, 2012

Fluorine-doping on the $Li_{1+x}Mn_{1.9-x}Al_{0.1}O_4$ spinel cathode materials is found to alter crystal shape, and enhance initial interfacial reactivity and solid electrolyte interphase (SEI) formation, leading to improved initial coulombic efficiency in the voltage region of 3.3-4.3 V *vs.* Li/Li^+ in the room temperature electrolyte of 1 M $LiPF_6$/EC:EMC. SEM imaging reveals that the facetting on higher surface energy plane of (101) is additionally developed at the edges of an octahedron that is predominantly grown with the most thermodynamically stable (111) plane, which enhances interfacial reactivity. Fluorine-doping also increases the amount of interfacially reactive Mn^{3+} on both bulk and surface for charge neutrality. Enhanced interfacial reactivity by fluorine-doping attributes instant formation of a stable SEI layer and improved initial cyclic efficiency. The data contribute to a basic understanding of the impacts of composition on material properties and cycling behavior of spinel-based cathode materials for lithium-ion batteries.

Key Words : Spinel cathode, Fluorine-doping, Interfacial reactivity, SEI formation, Lithium-ion batteries

Introduction

The $LiMn_2O_4$-based spinels are one of the most promising cathode materials for high power lithium-ion batteries for electric vehicles and energy storage systems because of their low cost, safety, environmental benignity and excellent rate capability.[1] The local structural distortion of MnO_6 octahedron by Jahn-Teller effect of Mn^{3+} and its disproportionation to Mn^{4+} and Mn^{2+} at the spinel surface [2-4] and the facile Mn^{2+} solvation by carbonate solvents[5] are recognized as the causes for Mn^{2+} dissolution, structural degradation and performance fade. The presence of HF acid in the $LiPF_6$-containing liquid electrolyte is noticed to trigger the extraction of Mn^{2+} and Li^+ ions. This interfacial reactions occurring in the early stage of cycling results in lowering of initial coulombic efficiency and performance fade, which is intensified at elevated temperatures. Cationic substitution (*e.g.* Li, Al) for Mn, which induces the increase in Mn^{4+} content, improved structural stability and cycling performance.[6-8] Our earlier work showed that surface Mn^{4+}-abundance on the Li-, and Al-doped spinel permits the formation of a stable SEI layer while being reduced to Mn^{3+} during early cycling.[9] Building-up of a stable SEI layer at the cathode surface during early cycles before the occurrence of Mn^{2+} dissolution is an effective approach toward enhanced operating cycle life.

Anionic substitution with fluorine for oxygen, which forms spinel oxyfluorides, together with cationic substitution improved cycling ability in the 4 V region despite the increase in Mn^{3+} content.[10-12] Amatucci *et al.* explained that the performance enhancement was associated with resistance of oxyfluorides to the HF attack.[13] The higher ionicity of the Mn-F bond than Mn-O bond might result in lowering of Mn^{3+} ion mobility, and therefore lowering reactivity towards dissolution. Yonezawa *et al.* reported that surface fluorination of $LiMn_2O_4$ by F_2 gas treatment resulted in higher cycling efficiency (≤ 95%) than untreated one.[14] Other relevant reports showed that a small fraction of F-substitution for O atom of 5 V $LiMn_{1.5}Ni_{0.5}O_{4-y}F_y$ ($y \leq 0.1$) could reduce Ni- and Mn-dissolution, improving capacity retention and thermal stabilities.[15,16] Similar results were reported by He *et al.* for the surface F-doping (≤ 5%) on $Li_{1.15}Mn_{1.85}O_4$.[17] Although the effects of cationic and anion substitution on the cycling performance of spinel cathodes have been extensively studied, the concrete conclusions of fluorine-substitution or doping effect on interfacial reaction behavior and their correlation to cycling behavior have not been clearly understood. In particular, in the absence of carbon-coating or surface modification on cathode, and electrolyte additive, initial coulombic efficiency of spinel cathode often remains low. Nonetheless, little attention is paid on the issue of initial cycling behavior and the SEI formation.

In the present paper, we focus on a basic understanding of the roles of fluorine-doping in enhancing initial cycle efficiency and the SEI formation of the Li-, and Al-cosubstituted $LiMn_2O_4$ spinel cathodes, using *ex situ* attenuated total reflectance Fourier transform infrared (ATR FTIR) spectroscopy.

Experimental

Two types of active materials of $Li_{1+x}Mn_{1.9-x}Al_{0.1}O_4$ spinels with fluorine-doping (denoted as D1 and D2 henceforth) and undoped counterparts (U1 and U2), synthesized using MnO_2 and lithium salt using a spray drying followed by calcination at 850-900 °C in air and slow cooling, were provided by POSCO ES Materials. For the synthesis of fluorine-doped D1 and D2 materials, LiF was used as a fluorine source. Table 1 presents the notation, composition, crystal structural information and the relative ratio of bulk and surface Mn valences of the active materials, determined by inductively coupled plasma-atomic emission spectroscopy (ICP-AES), X-ray diffraction (XRD) and a least-squares method for cell parameter refinement, and X-ray photoelectron spectroscopy (XPS), respectively. The XRD patterns were obtained using an X-ray diffractometer (Rigaku D/MAX-2200), which was measured from 15 to 65° 2θ with the scan rate of 1°/min at 0.02° step. The presence of doped fluorine (F) was confirmed with field emission scanning electron microscopy (SEM, JEOL JSM-7000F) imaging at 5 kV and energy dispersive X-ray (EDX) elemental mapping result as well as the variation of cell parameter from the undoped materials. XPS spectra were recorded with MultiLab 2000 with Al K_α X-ray source at the output power of 200 W under a pressure of 2.0×10^{-9} mbar. The irradiated spot size was about 320 μm and the pass energy was 20 eV. The binding energy was calibrated based on the C 1*s* level at 284.7 eV. The experimental peak shape of Mn $2p_{3/2}$ was modeled by employing multiple-splitting patterns derived for Mn^{2+}, Mn^{3+} and Mn^{4+} at 641.0, 641.7, and 642.7 eV from the standard compounds of MnO, Mn_2O_3 and MnO_2, respectively.[18] The Mn 2*p* spectra were fitted after correcting the baseline using the Shirley method till the goodness-of-fit down to about 1. Particle morphology was examined using SEM imaging.

Lithium cells containing spinel cathode as a working electrode were assembled with Li reference and counter electrodes, and a polypropylene separator (Celgard 2400) in 1 M $LiPF_6$/EC:EMC (volume ratio 3:7) electrolyte (Techno Semichem) in the glove box. The cathodes laminated on the Al current collector were composed of 94 wt % active material, 3 wt % carbon black and 3 wt % polyvinylidene difluoride (PVdF) binder. Galvanostatic cycling was conducted for five cycles between 3.3 and 4.3 V *vs.* Li/Li^+ at 100 $mAcm^{-2}$ (0.1C) using a multilchannel galvanostat (Won-A Tech).

Surface characterization for the cycled cathodes (unwashed) was performed using *ex situ* attenuated total reflection (ATR) FTIR spectroscopy using an IR spectrometer (Nicolet 6700) equipped with a MCT detector. In order to avoid washing-off event of soluble surface species during washing with dimethyl carbonate (DMC), the cathodes unwashed were subjected to IR analyses. Cycled cathodes were directly mounted on the tightly closed single-reflection ATR unit with a Ge optic in the Ar-filled glove box to avoid the exposure to the air. There was no moment of atmospheric contamination for the samples during transportation from glove box to dry N_2-purged sample compartment of the IR instrument as well as during IR measurement. The spectra were acquired with the spectral resolution of 4 cm^{-1} and total 512 scans co-added.

Results and Discussion

Characterization of Bulk and Surface Structures. The XRD patterns in Figure 1 reveal that all spinel active materials are crystallized in a cubic spinel structure (*Fd-3m*) as a single phase. Relative ratio of Mn^{3+}/Mn^{4+} for the bulk materials, determined from the normal formula of $Li_{1+x}Mn_{1.9-x}Al_{0.1}O_4$ (U1 and U2) and $Li_{1+x}Mn_{1.9-x}Al_{0.1}O_{3.99}F_{0.01}$ (D1 and D2), is listed in Table 1. For fluorine-free (U1 and U2) materials, overall the concentration of bulk Mn^{4+} is relatively higher (59-64%) than Mn^{3+} (36-41%). The Li content is slightly variable probably for charge neutrality,

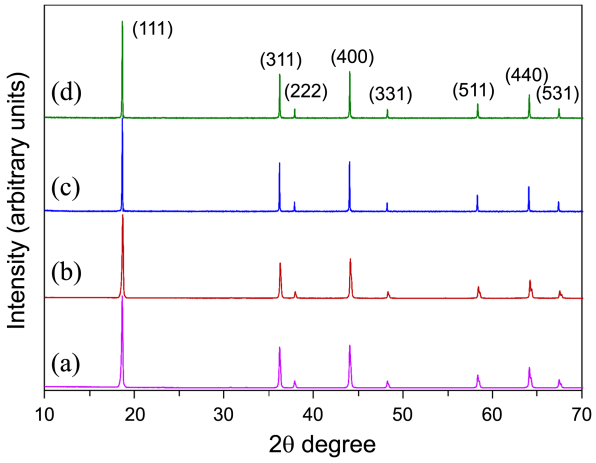

Figure 1. X-ray diffraction patterns of fluorine-free (a) U1 and (b) U2, and fluorine-doped (c) D1 and (d) D2 spinel active materials.

Table 1. Notation, composition, cell parameter, bulk and surface Mn valences, and initial cycling properties of Li, Al-cosubstituted spinel cathodes (U1 and U2) and with fluorine-doping (D1 and D2)

Cathode	Composition	Cell parameter (Å)	Bulk Mn^{4+}/Mn^{3+} ratio (%)[a]	Surface Mn^{4+}:Mn^{3+} ratio (%)	Initial discharge capacity ($mAhg^{-1}$)	Initial coulombic efficiency (%)
U1	$Li_{1.08}Mn_{1.83}Al_{0.09}O_4$	8.2097	64 : 36	100 : 0	102	86
U2	$Li_{1.01}Mn_{1.89}Al_{0.1}O_4$	8.2022	59 : 41	95 : 5	96	85
D1	$Li_{1.01}Mn_{1.89}Al_{0.1}O_{3.99}F_{0.01}$	8.2154	53 : 47	88 : 12	108	97
D2	$Li_{1.05}Mn_{1.84}Al_{0.11}O_{3.99}F_{0.01}$	8.2138	59 : 41	91 : 9	113	98

[a]Calculated from the composition

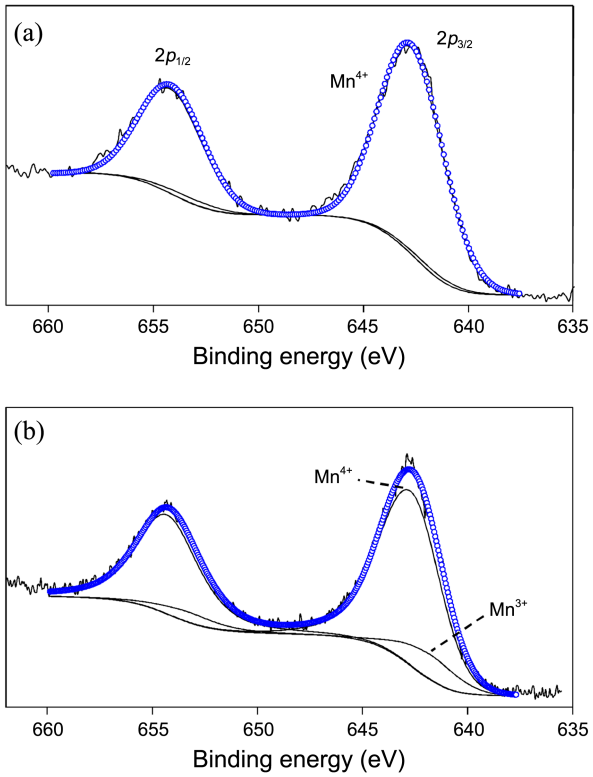

Figure 2. X-ray photoelectron spectra of (a) fluorine-free U1 and (b) fluorine-doped D1 spinel active materials.

and average Mn valence and cell parameter are variable accordingly. Cell parameters for fluorine-doped materials are larger than those of undoped ones. This is opposite to Vegard's rule for the substitution of fluorine with smaller ionic radius (1.33 Å) for oxygen (1.40 Å),[19] The increase in cell parameter by fluorine-doping is thus attributed to the increase in the amount of Mn^{3+} with larger ionic radius (0.645 Å) than that of Mn^{4+} ion (0.53 Å)[19] for charge compensation, which is consistent with relatively larger Mn^{3+} content for fluorine-doped materials in Table 1.

Surface Mn valance was determined using curve fitting on the Mn 2*p* spectral peaks as shown in Figure 2. Table 1 compares the average surface Mn valence determined from fitting results. The surface of undoped spinel cathode materials (U1 (Fig. 2(a)) and U2) consist of 95-100% Mn^{4+} (Table 1), which have relatively oxygen-abundant and lithium-lean surface. For the fluorine-doped materials (D1 (Fig. 2(b)) and D2), the Mn^{4+} content becomes relatively lower (88-91%) as shown in Table 1. This reveals that fluorine-doping affects not only on the bulk Mn valence but also surface, lowering surface oxygen content but increasing Li^+ content.

Crystal Shape. Figure 3 compares the shape of a primary particle of U1 and D1, which are picked for comparison. Primary particles are 2-3.5 μm in size. The particle of U1 (Fig. 3(a)) has a sharp-edged octahedron shape with additional small area facets on the top and bottom, which correspond to facetting predominantly on the (111) and (001) planes, respectively, referred to TEM analysis results for $LiMn_2O_4$ crystals.[20] The surface energy of lattice planes for a

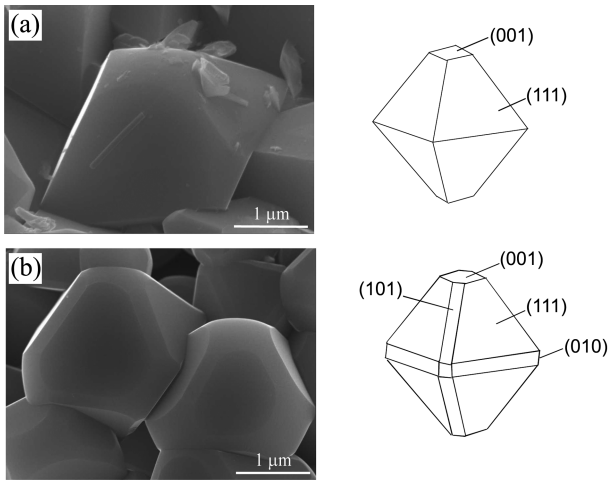

Figure 3. SEM images for primary particles of (a) U1 and (b) D1 active materials, and the schematics of their crystal shape.

$LiMn_2O_4$ crystal was predicted as the increasing order of (111) < (110) < (100).[20] This indicates that the particle of U1 grows dominantly on the most thermodynamically stable lattice plane of (111). Upon fluorine-doping (Fig. 3(b)), particle shape tends to maintain but new narrow facets on the edges referred to (101) plane are developed. Fluorine-doping alters a growth habit of spinel particle a bit by permitting the formation of (101) facets, probably by a kinetic control. However the presence of (101) plane is not reflected in the XRD pattern in Figure 1(c)-(d) due to its small fraction and low detection limit of XRD. It is estimated that the exposure of such higher surface energy plane to electrolyte increases initial interfacial reactivity and affect the kinetics of SEI formation.

Initial Cycling Behavior. The lithium cells with spinel cathodes were tested for their initial cycling behavior using constant current cycling at ~C/10 rate between 3.3 and 4.3 V. Figure 4(a)-(b) exhibit the voltage profiles of U1 and D1 cathodes, respectively. For both cathodes, the initial cycle curve shows two prominent anodic plateaus near 4.04 and 4.15 V due to stepwise lithium deintercalation, together with cathodic plateaus at 4.01 and 4.12 V by lithium intercalation, respectively. Fluorine-doped materials (D1 and D2) provide slightly larger initial charge capacities of 112 and 115 $mAhg^{-1}$ (Table 1) respectively, than 106 and 113 $mAhg^{-1}$ for U1 and U2, respectively. The reason for the capacity enhancement of fluorine-doped spinel is due to increased amount of Mn^{3+} ions that are subjected to oxidation upon Li^+ deintercalation. Figure 4(c) shows significantly enhanced initial efficiencies of D1 and D2 to 97-98%, in contrast to 85-86% of U1 and U2, although inferior initial coulombic efficiencies are predicted for D1 and D2 by the presence of more amounted Mn^{3+} for the disproportionation to Mn^{2+} and Mn^{4+} and high surface energy (101) plane. This means that the tendency of electrolyte oxidation at D1 and D2 cathodes during initial charging decreases, compared to U1 and U2. Electrolyte may already undergo oxidation just by contact with interfacially reactive fluorine-doped cathode during

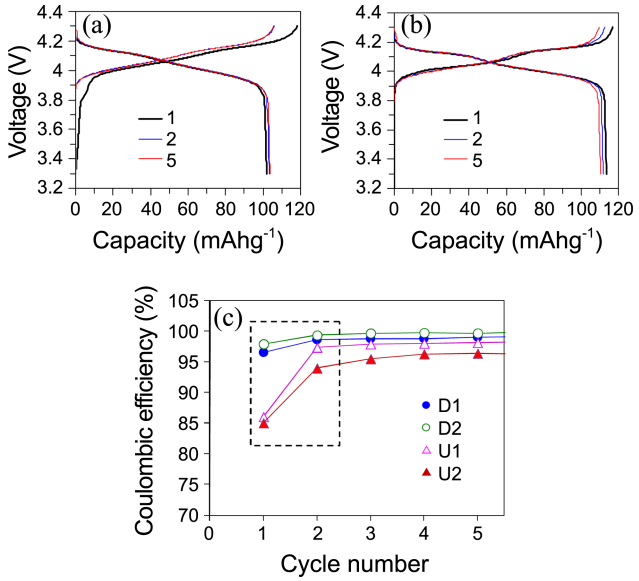

Figure 4. Voltage profiles of lithium cells with the spinel cathodes of (a) U1 and (b) D1, and plots of (c) Coulomb efficiencies for five cycles in the room temperature electrolyte of 1M $LiPF_6$/EC:EMC.

wetting leading to the SEI formation.

Characterization of the SEI Layer on Cycled Cathodes. The effects of fluorine-doping on the SEI formation and composition of the spinel cathodes are investigated using *ex situ* ATR FTIR spectroscopy. Figure 5(a) shows the IR spectra of U1 and D1 cathodes that underwent 5 cycles, together with pristine D1 and electrolyte residue as references. Cycled cathodes were subjected to the IR measurement as unwashed. Note that IR active bands of spinel $LiMn_2O_4$ material are observed below 700 cm^{-1}, which is out of our mid-IR spectral range.[21]

Spectrum of pristine cathode (Fig. 5(a)-(i)) shows prominent peaks characteristic of PVdF binder. The spectra of cycled cathodes in Figure 5(a)-(b) reveal new peaks distinguished from those of PVdF and electrolyte residue. The D1 cathode reveals significantly strong (eight times) peaks absorbance compared to U1. This is the direct evidence of higher surface coverage by the SEI layer and SEI thickening on fluorine-doped cathode. As predicted, promoted interfacial reactivity pertaining to D1 might facilitate the formation of the SEI layer during wetting and further accumulation of the SEI compounds during 5 cycles.

Prominent peaks at 2975-2854 cm^{-1} (Fig. 5(a)-iii, iv) together with fingerprints for both cycled cathodes are characteristic of CH_3- methyl and -CH_2- methylene of alkyl group.[22] A tiny new peak at 3005 cm^{-1} is associated with the methylene group bonded to the electronegative substituent (*e.g.* F) and methylene group of EC ring. Also shown are two prominent bands at 1808 and 1776 cm^{-1} (Fig. 5(b)) with other fingerprints, characteristic of C=O group of the EC for the EC:$LiPF_6$ solvate from electrolyte residue.[9,23,24] Magnified spectra (Fig. 5(b)) for the C=O stretching region clearly displays an appearance of two new couple of peaks at 1819 and 1756 cm^{-1}, and 1778 and 1770 cm^{-1} on both U1 and D1 cathodes

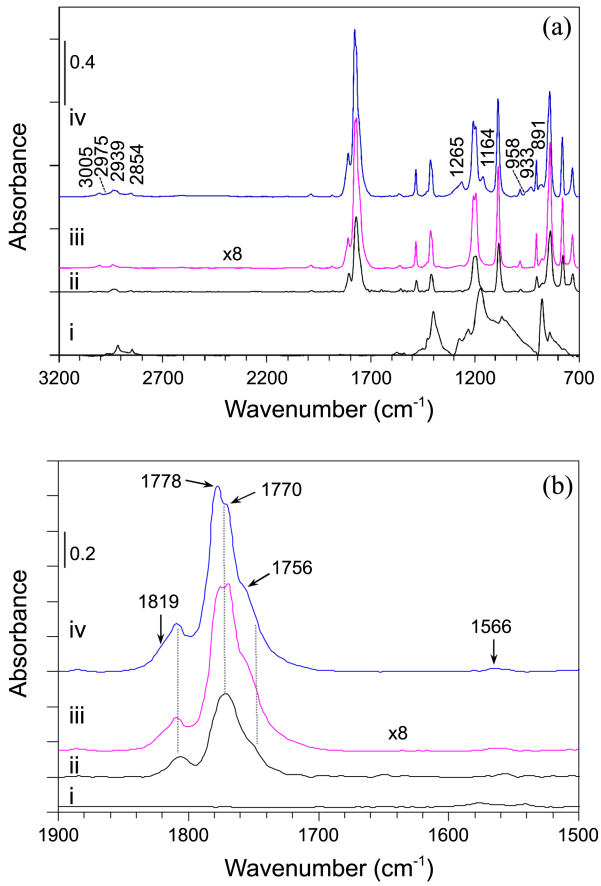

Figure 5. IR spectra for the surface of (i) pristine D1 cathode, (ii) electrolyte residue, and cycled cathodes of (iii) U1 and (iv) D1 unwashed in the regions of (a) 4000-700 cm^{-1} and (b) 1900-1500 cm^{-1}.

(Fig. 5(b)-iii, iv). They are attributed to anhydride -CO-O-CO- and ester -CO_2R (R = alkyl) functionalities,[9,23,24] respectively. High wavenumber of ester reflects the presence of electronegative substituent (*e.g.* F).[23] The overlapped peaks near 1265 and 1080 cm^{-1} due to C-O-C and O-C-C stretchings confirm the presence of ester compound. The surface of cycled D1 exhibits additional tiny peak at 1566 cm^{-1}, attributed to carboxylate salts -$CO_2^-M^{n+}$ (M = Li/Mn).[9,23] Such new organic SEI compounds should be the decomposition products of organic carbonates (EC, EMC) and their derivatives. The D1 (Fig. 5(a)-iv) also exhibits low absorbance peaks at 1265, 1164 and 1016 cm^{-1}, due to P=O and P-O-C groups, and the one near 891 cm^{-1} by P-F functionality.[23] They are attributed to organic phosphorus fluoride compounds, (OR)FP=O and PF-containing species.[9,23,25] As the $LiPF_6$ is in equilibrium with PF_5 and LiF and is subjected to hydrolysis in the presence of humidity, the presence of PF-containing surface species on D1 surface provides indirect evidence that LiF salt is also forms on the surface. The LiF is not observable in the mid-IR (4000-700 cm^{-1}) region. On the contrary, the low wavenumber peaks are hardly observed on the U1 (Fig. 5(a)-iii).

The IR analysis results reveal that the surface of cycled D1 cathode is effectively passivated by significantly thicker SEI

layer than U1. The SEI layer of D1 is composed of organic compounds including anhydride, ester and carboxylate salt functionalities, and organic phosphorus-fluorine compound and PF-containing inorganic species, which are produced by oxidative decomposition of EC and EMC solvents, and $LiPF_6$ salt, respectively. On the contrary, just organic compounds at a relatively very low concentration are detected on the surface of U1. Instant formation of the SEI layer on D1 cathode during wetting and initial cycling due to increased interfacial reactivity by fluorine-doping and subsequent effective surface passivation attributes enhancement of initial coulombic efficiency (Fig. 5(c)).

Conclusions

Roles of fluorine-doping in enhancing the initial cycle efficiency and SEI formation of Li- and Al-cosubstituted spinel cathodes have been investigated. Fluorine-doping on spinel cathode results in the formation of higher surface energy plane of (101) in addition to thermodynamically stable (111) plane and an increase of relative amount of Mn^{3+} for charge neutrality, which promotes interfacial reactivity. As a result, fluorine-doping is found to facilitate instant and effective surface passivation with a stable SEI layer during wetting and initial cycling, resulting in enhanced initial coulombic efficiency to ≥ 97%. IR spectroscopic analysis data indicate that the SEI consists of the mixture of organic compounds of anhydride, ester and carboxylate salt, and inorganic compounds such as organic phosphorous compound and PF-containing species. The interfacial and electrochemical processes are estimated to occur in a more intense way at elevated temperatures, which would be reported in the forthcoming paper. Effective passivation of cathode surface is believed to be necessary in improving cycle life of lithium-ion batteries employing spinel-based cathodes.

Acknowledgments. This work was supported by a grant from the Fundamental Materials & Components Technology Developing Program of Knowledge & Economy.

References

1. Ohzuku, T.; Kitagawa, M.; Hirai, T. *J. Electrochem. Soc*. **1990**, *137*, 769.
2. Hunter, J. C. *J. Solid State Chem*. **1981**, *39*, 142.
3. Gummow, R. J.; Kock, A. de; Thackeray, M. M. *Solid State Ionics* **1994**, *69*, 59.
4. Tarascon, J.-M.; Coowar, F.; Amatucci, G. G.; Shokoohi, F. K.; Guyomard, D. G. *J. Power Sources* **1995**, *54*, 103.
5. Son, H.-Y.; Lee, M.-Y.; Ko, H.-S.; Lee, H. *J. Korean Electrochem. Soc*. **2011**, *14*, 131.
6. Myung, S.-T.; Komaba, S.; Kumagai, N. *J. Electrochem. Soc*. **2001**, *148*, A482.
7. Bakenov, Z.; Taniguchi, I. *Solid State Ionics* **2005**, *176*, 1027.
8. Xia, Y.; Zhang, Q.; Wang, H.; Nakamura, H.; Noguchi, H.; Yoshio, M. *Electrochim. Acta* **2007**, *52*, 4708.
9. Song, J.-W.; Nguyen, C. C.; Choi, H.; Lee, K.-H.; Han, K.-H.; Kim, Y.-J.; Choy, S.; Song, S.-W. *J. Electrochem. Soc*. **2011**, *158*, A458.
10. Kang, Y.-J.; Kim, J.-H.; Sun, Y.-K. *J. Power Sources* **2005**, *146*, 237.
11. Choi, W.; Manthiram, A. *Solid State Ionics* **2007**, *178*, 1541.
12. Feng, C.; Li, H.; Zhang, C.; Guo, Z.; Wu, H.; Tang, J. *Electrochim. Acta* **2012**, *61*, 87.
13. Amatucci, G. G.; Pereira, N.; Zheng, T.; Tarascon, J.-M. *J. Electrochem. Soc*. **2001**, *148*, A171.
14. Yonezawa, S.; Yamasaki, M.; Takashima, M. *J. Fluorine Chem*. **2004**, *125*, 1657.
15. Oh, S. W.; Park, S. H.; Kim, J. H.; Bae, Y. C.; Sun, Y. K. *J. Power Sources* **2006**, *157*, 464.
16. Stroukoff, K. R.; Manthiram, A. *J. Mater. Chem*. **2011**, *21*, 10165.
17. He, X.; Li, J.; Cai, Y.; Wang, Y.; Ying, J.; Jiang, C.; Wan, C. *Solid State Ionics* **2005**, *176*, 2571.
18. NIST X-ray Photoelectron Spectroscopy Database, NIST Standard Reference Database 20, version 3.5. http://srdata.nist.gov/xps/ (accessed July 2012).
19. Shannon, R. D. *Acta Cryst. A* **1976**, *32*, 751.
20. Huang, M.-R.; Lin, C.-W.; Lu, H.-Y. *Appl. Surf. Sci*. **2001**, *177*, 103.
21. Rougier, A.; Striebel, K. A.; Wen, S. J.; Richardson, T. J.; Reade, R. P.; Cairns, E. J. *Appl. Surf. Sci*. **1998**, *134*, 107.
22. Socrates, G. *Infrared Characteristic Group Frequencies*, 2nd ed.; John Wiley & Sons: New York, 1994.
23. Zhuang, G. V.; Ross, P. N., Jr. *Electrochem. Solid-State Lett*. **2003**, *6*, A136.
24. Song, S.-W.; Zhuang, G. V.; Ross, P. N., Jr. *J. Electrochem. Soc*. **2004**, *151*, A1162.
25. Yang, H.; Zhuang, G. V.; Ross, P. N., Jr. *J. Power Sources* **2006**, *161*, 573.